DR DANIEL F CUTLER (Orcid ID : 0000-0002-4288-7530)

Article type : Original Article

Modulation of endothelial organelle size as an antithrombotic strategy

Francesco Ferraro[1,4,§*], Francesca Patella[1§], Joana R. Costa[2,5], Robin Ketteler[2], Janos Kriston-Vizi[3], Daniel F. Cutler[1*]

[1] Endothelial Cell Biology Group, MRC Laboratory for Molecular Cell Biology, University College London, Gower Street, London, WC1E 6BT

[2] Cell Signalling and Autophagy Group, MRC Laboratory for Molecular Cell Biology, University College London, Gower Street, London, WC1E 6BT

[3] Bioinformatics Image Core (BIONIC), MRC Laboratory for Molecular Cell Biology, University College London, Gower Street, London, WC1E 6BT

[4] Current address, Department of Biology and Evolution of Marine Organisms (BEOM), Stazione Zoologica Anton Dohrn, Villa Comunale, 80121 Naples

[5] Current address, Leukaemia Biology Research Group, Department of Haematology, Cancer Institute, University College London, 72 Huntley Street, London, WC1E 6DD

§ Equal contribution

*Corresponding authors

This article has been accepted for publication and undergone full peer review but has not been through the copyediting, typesetting, pagination and proofreading process, which may lead to differences between this version and the Version of Record. Please cite this article as doi: 10.1111/JTH.15084

Daniel F. Cutler
MRC Laboratory for Molecular Cell Biology, University College London,
Gower Street, London, WC1E 6BT
United Kingdom
Phone: +44 (0)20 7679 7808
Email: d.cutler@ucl.ac.uk

Francesco Ferraro
Department of Biology and Evolution of Marine Organisms (BEOM), Stazione Zoologica Anton Dohrn, Villa Comunale, 80121 Naples, Italy
Phone: +39 081 5833301
Email: francesco.ferraro@szn.it

Essentials

- Endothelial Von Willebrand Factor (VWF) stored in specific secretory granules (Weibel-Palade bodies, WPBs) is central to haemostasis and thrombosis.
- VWF secretion from shorter secretory granules shows dramatically reduced primary haemostatic activities.
- Shortening WPBs thus represents a novel opportunity to modulate haemostatic activity and reduce thrombotic risk.
- Screening licensed drugs for WPB-shortening activity reveals a set of potential anti-thrombotic compounds.

Summary

Background

It is long-established that Von Willebrand Factor (VWF) is central to haemostasis and thrombosis. Endothelial VWF is stored in cell-specific secretory granules, Weibel-Palade bodies (WPBs), organelles generated in a wide range of lengths (0.5 to 5.0 μm). WPB size responds to physiological cues and pharmacological treatment, and VWF secretion from shortened WPBs dramatically reduces platelet and plasma VWF adhesion to an endothelial surface.

Objective

We hypothesised that WPB-shortening represented a novel target for antithrombotic therapy. Our objective was to determine whether compounds exhibiting this activity do exist.

Methods

Using a microscopy approach coupled to automated image analysis, we measured the size of WPB bodies in primary human endothelial cells treated with licensed compounds for 24 h.

Results and Conclusions

A novel approach to identification of antithrombotic compounds generated a significant number of candidates with the ability to shorten WPBs. In vitro assays of two selected compounds confirm that they inhibit the pro-haemostatic activity of secreted VWF. This set of compounds acting at a very early stage of the haemostatic process could well prove to be a useful adjunct to current antithrombotic therapeutics. Further, in the current SARS-CoV-2 pandemic, with a considerable fraction of critically ill COVID-19 patients affected by hypercoagulability, these WPB size-reducing drugs might also provide welcome therapeutic leads for frontline clinicians and researchers.

Keywords.

Von Willebrand Factor; Weibel-Palade bodies; Thrombosis ; Drug repurposing; COVID-19.

Introduction

Endothelial Von Willebrand Factor (VWF) plays a fundamental role in haemostasis, with deficiencies in its activity causing von Willebrand Disease (VWD), the most common inherited human bleeding disorder [1]. VWF is a large multi-domain glycoprotein, whose function in haemostasis depends on its multimeric status. VWF multimers act as mechano-transducers, which respond to shear forces in the circulation by stretching open and exposing binding sites for

integrins, collagen, platelets and homotypic interaction (i.e., between VWF multimers) [2]. Endothelial cells secrete VWF in a highly multimerized form, known as ultra-large (UL)-VWF, extremely sensitive to haemodynamic forces and thus very active in platelet binding [3].

UL-VWF's potential to cause spontaneous thrombus formation is controlled by a circulating protease, ADAMTS13, which generates the less-multimerised, less active forms of VWF seen in plasma [3]. Persistence of UL-VWF in the circulation leads to microvascular thrombosis and the highly morbid and potentially life threatening clinical manifestations observed in a host of infectious and non-infectious diseases, such as sepsis and thrombotic thrombocytopenic purpura (TTP)[4, 5]. Although these may be the most extreme examples of excess VWF function, many common disorders including hypertension and diabetes are characterised by increased VWF plasma levels [6, 7].

While VWF is stored in the secretory granules of both platelets and endothelial cells, most of the VWF circulating in plasma derives from endothelial WPBs and is fundamental to haemostasis [8, 9]. Vessel injury, in either the macro- or microcirculation, triggers localized stimulated exocytosis of WPBs, mediated by a variety of agonists [10]. UL-VWF secreted from activated endothelium forms cable-like structures built of multiple multimers, both in vitro and in vivo [11, 12]. These VWF "strings" provide scaffolds for the recruitment of circulating platelets and soluble plasma VWF, contributing to the formation of the primary haemostatic plug, but also potentially promoting microangiopathy [2, 13].

The length of VWF strings generated upon exocytosis reflects the size of the WPBs in which VWF was stored. WPBs are cigar-shaped organelles, whose length ranges ten-fold, between 0.5 and 5.0 μm. Their size depends on the structural status of the endothelial Golgi apparatus where they form, and experimental manipulations causing Golgi fragmentation consistently result in the formation of only short WPBs [14]. Short WPBs also form when VWF biosynthesis by endothelial cells is reduced, or following statin treatment, via Golgi fragmentation-independent and –dependent mechanisms, respectively [14, 15]. Organelle size is also regulated by the metabolic status of endothelial cells, through an AMPK/GBF1-mediated signalling pathway [16] and, transcriptionally, by up-regulation of KLF2 [17].

Importantly, *in vitro* experiments have revealed that reducing WPB size results in the shortening of the VWF strings they generate and in much-reduced recruitment of platelets and soluble circulating VWF to the endothelial surface [14, 15]. Conversely, endothelial cells respond to raised glucose levels (mimicking hyperglycemia) by producing longer WPBs, suggesting a link

between long VWF strings and thrombotic manifestations in diabetes [16], which is often associated with high levels of plasma VWF and microangiopathy [7].

WPB size is, therefore, plastic and responds to physiological cues and pharmacological treatments. Such findings suggest that drug-mediated reduction of WPB size might provide alternative or coadjuvant therapeutic approaches to current clinical interventions in thrombotic pathologies where dysregulated formation and/or prolonged persistence of VWF strings on vascular walls play a triggering role.

We designed a screen to identify drugs that reduce WPB size and thus can potentially reduce endothelial pro-thrombotic capacity. Out of 1280 human licensed drugs we found 37 compounds fitting our criteria, with a variety of mechanisms of action, implying that a number of cellular pathways influence biogenesis of WPBs.

Results.

Screen. A quantitative high-throughput microscopy-based workflow, dubbed high-throughput morphometry (HTM), allows rapid quantification of the size of tens to hundreds of thousands of WPBs within thousands of endothelial cells [14]. HTM has been applied for analytical purposes and in phenotypic screens [14-16, 18-20]. In the present report, HTM was deployed to identify compounds that can induce a reduction of WPB size in Human Umbilical Vein Endothelial Cells (HUVECs). In cultured HUVECs, WPBs longer than 2 μm account for approximately 20% of these organelles and roughly 40% of the VWF they store [14]. Thus, while a minority, these long WPBs are disproportionally important with respect to secreted endothelial VWF. For the purpose of the screen, we quantified WPB size as the ratio between the area covered by WPBs longer than 2 μm and the area covered by all these organelles; we define this parameter as "fractional area (FA) of long WPBs" (**Figure 1A)** [15]. The effect of each compound in the library on WPB size was compared to two controls: treatment with DMSO and Nocodazole, the negative and positive controls, respectively, for WPB shortening [14, 15] (**Figure 1B, 1C**). HUVECs were incubated with the 1280 compounds of the Prestwick library at 10 μM for 24 h in single wells of 96-well plates, in duplicate (two separate plates; **Figure 1D**). After fixation, immuno-staining and image acquisition, the FA of long WPBs in treated cells was quantified. Per plate and inter-plate normalization to DMSO-controls was implemented in order to rank the effects of the library compounds on WPB size by Z-score, (**Figure 1E; Table S1**).

Hit selection and confirmation. Statins are cholesterol-lowering drugs that inhibit the enzyme 3-hydroxy, 3-methylglutaryl CoA reductase (HMGCR) in the mevalonate pathway, upstream of the biosynthesis of cholesterol. We have previously shown that treatment of endothelial cells with two statins, simvastatin and fluvastatin, induces WPB size shortening, resulting in reduced adhesive properties of the VWF released by activated endothelial cells (HUVEC), measured by the reduced size of platelet-decorated VWF strings and by the recruitment of VWF from a flowing plasma pool [15]. Fluvastatin and simvastatin are present in the Prestwick library. We therefore used their Z-score to establish a stringent cut-off for selection of positive hits. This approach identified 58 compounds, 4.5% of the library (**Figure 1E,** orange box, simvastatin and fluvastatin).

Concentration-response experiments were then carried out in order to both confirm compound activity and establish their EC_{50} or minimal effective concentrations. HUVECs were incubated for 24 h with the 58 hits at concentrations ranging from 10 μM to 78 nM (**Figure 1F**). Following image analysis, if the fractional area of long WPBs was ≤ 0.35, at least at 10 μM, compounds were confirmed as WPB-shortening. This secondary screen confirmed that 37 licenced compounds (2.9% of the library) are capable of inducing WPB size reduction in 24 h, with varied potency (**Table 1**). Of note, aside from simvastatin and fluvastatin, the other three statins present in the Prestwick library were confirmed as WPB-shortening drugs (**Table 1**), indicating that both our screening approach and the criteria for hit selection were robust.

Compound pharmacology. A survey of the mechanisms of action of the 37 compounds showed that they had diverse pharmacology, consistent with the existence of a variety of mechanisms of WPB size control (**Table S2**). Based on their primary target or the biological activity affected, 26 drugs could be allocated into eight pharmacological classes, each with at least two compounds (**Table 1; Table S2; Figure 2**). Considering other known molecular targets of all the compounds and the cellular processes they that affect, five additional classes were identified. Several compounds were shared among pharmacological classes (**Table 1; Table S2; Figure 2A**).

Among the pharmacological classes inducing WPB shortening, we found microtubule (MT) depolymerizing agents, histone deacetylase (HDAC) inhibitors, topoisomerase inhibitors and, as mentioned earlier, statins (HMGCR inhibitors). Compounds with these mechanisms of action have been shown induce unlinking of the ribbon architecture of the Golgi apparatus, i.e. Golgi "fragmentation" [15, 21-23]. Since an intact Golgi ribbon is required for the biogenesis of long WPBs [14] (see, for instance, nocodazole in **Figure 1B**), identification of these classes of

molecules in our screen was expected. Previous work from our lab also showed that neutralization of the acidic lumen of WPBs disrupts the tubular structure of VWF, shifting the organelle shape from cylindrical to spherical, which is detected as shortening [24]; and indeed we identified trans-membrane pH gradient depleting agents. Reduction in VWF biosynthesis results in shorter WPBs without affecting the Golgi architecture [14] and one of the screen hits, cycloheximide, is a classic protein synthesis inhibitor, while other compounds identified here have also been reported to have this activity (**Figure 2B**) [25].

Aside from those expected examples, entirely novel WPB-shortening drug classes were also identified, including estrogen, glucocorticoid, serotonin and histamine receptor agonists or antagonists, noradrenaline reuptake inhibitors and cardiac glycosides. Many of the identified compounds are shared by two or more pharmacological classes (**Figure 2A**), which may signal that these compounds mediate their effects on WPB size through yet unidentified common cellular processes and signalling pathways. In this respect, it is interesting that several compounds are also substrates and inhibitors of multidrug resistance protein 1, MDR1/ABCB1 (**Table 1; Table S2; Figure 2A**), an activity that may therefore hint at one of the cellular pathways that regulate WPB size.

The cardiac glycosides and their cardenolide precursors were prominent among these novel pharmacological classes. These molecules, which inhibit Na^+/K^+-ATPase (**Table 1** and **Table S2**), have a long clinical history in the treatment of congestive heart failure and atrial fibrillation and have recently attracted interest as potential anticancer molecules [26] and senolytics, i.e., selective inducers of senescent cell death [27]. As a class, cardiac glycosides and cardenolides display the strongest WPB-shortening activity (**Figure 2B**) and induce Golgi apparatus compaction (**Figure 3A**) instead of its fragmentation, suggestive of a novel WPB size-reducing mechanism. In most cases, sub-micromolar concentrations of these compounds were sufficient to reduce WPB size, with proscillaridin A being effective at low nanomolar concentrations (**Figure 3B; Table 1**).

Hit validation. We have shown that VWF exocytosis results in homotypic recruitment of the soluble VWF pool present in plasma to the stimulated endothelial surface and that treatments which reduce WPB size inhibit this process [15]. We therefore tested whether novel compounds identified in our screen had this same effect. Cardiac glycosides and their aglycone precursors display a steep concentration/activity curve, meaning that their WPB-shortening activity remains maximal down to and immediately disappears below their EC_{50} (**Figure 3B**). We therefore tested

the effects of the most active of these compounds, proscillaridin A, at 40 nM, a concentration ~ twofold higher than its EC_{50}. (**Figure 3B**). Treatment of HUVECs with proscillaridin at this concentration resulted in strong WPB-shortening, whose exocytosis generated, when compared to controls, reduced recruitment of plasma VWF (**Figures 4A-a** and **4A-f**). Since cardiac glycosides have been reported to inhibit protein synthesis [25], we assessed whether this might explain, through reduced VWF translation, their effect on WPB size. Protein and VWF levels in proscillaridin treated cells were reduced when compared to DMSO controls, although to different extents. VWF reduction (by ~ 50%), which was reflected not only in reduced WPB size but also by a fall in their numbers, was greater than the drop (by ~ 30%) in protein content (**Figure 4A-b, 4A-d** and **4A-e**). At 40 nM, proscillaridin did not affect cell numbers (**Figure 4A-c**), likely because in our experiments drug incubation started at 24 h after seeding, allowing cells to become confluent and stop dividing. Interestingly, this finding indicates that this concentration of proscillaridin is not toxic to cells, in contrast to what we find with other drugs identified in our screen when tested at high concentration (**Figure S1A** and **S1B**).

In a similar set of experiments, we also tested another novel WPB size-reducing compound, cyclosporine A, an inhibitor of the protein phosphatase calcineurin, clinically used as an anti-rejection drug in organ transplantation (**Table S1**) [28]. In contrast to cardiac glycosides, cyclosporine displays a more graded concentration-dependent effect on WPB size (**Figure S1C**). We have documented that statin treatment at concentrations exerting submaximal effects on WPB size nevertheless result in decreased adhesive VWF activity [15]. To verify whether this is a general feature of WPB size reduction, we tested cyclosporine at 1 μM, approximately its EC_{50} (**Table 2**). At this concentration, cyclosporine induced a moderate reduction in WPB size (**Figure 4B-a**); nevertheless, this size reduction was still efficient in diminishing soluble plasma VWF recruitment to the endothelial surface (**Figure 4B-f**). Cyclosporine had no effect on the number of cells, total protein or VWF levels (**Figure 4B-d** through **4B-e)**.

Discussion

Upon exocytosis, endothelial UL-VWF self-assembles into strings, which serve as recruiting platforms for platelets and circulating VWF, thus promoting the formation of the primary haemostatic plug [15, 29, 30]. VWF strings also mediate pathological processes such as tumour

metastasis, endocarditis and microangiopathies [13, 31, 32]. Interventions reducing the persistence and/or activity of VWF-strings are therefore of interest as potential anti-thrombotic therapies.

Modulation of organelle size has been suggested as a potential strategy to regulate biological functions and correct pathological states [33]. In this perspective, WPBs represent a paradigmatic example. Reduction of WPB size has no effect on UL-VWF formation, but blunts generation of long platelet-decorated VWF-strings following exocytosis and diminishes recruitment of plasma VWF to the endothelial surface [14, 15]. Interventions that shorten WPBs could therefore provide alternative or coadjuvant therapies to current clinical interventions in thrombotic pathologies where dysregulated formation and/or prolonged persistence of VWF-strings play a triggering role.

In addition to the pharmacological and experimental manipulations disrupting the integrity of the Golgi apparatus [14, 15], formation of short WPBs is mediated by endogenous signalling pathways. We have uncovered a pathway involving AMPK-dependent regulation of the Arf-GEF GBF1, which is independent of alterations in the structure of the Golgi apparatus and links WPB size to the metabolic status of endothelial cells [16]. Small WPBs are also generated upon overexpression of the transcription factor KLF2 [17]. KLF2 expression is promoted by athero-protective flow patterns and induces transcriptional changes in hundreds of endothelial genes, resulting in anti-inflammatory and antithrombotic cellular adaptations [34-37]. Treatment with statins also up-regulates KLF2 expression; and their anti-inflammatory, anti-coagulant and antithrombotic effects are believed to be mediated by this transcription factor [38, 39]. However, WPB size reduction induced by statin treatment does not require KLF2 [15]. Altogether, a significant body of experimental evidence indicates that the size of WPBs is subject to regulation and represents a target for pharmacological intervention in haemostatic function and thrombotic risk.

We therefore screened licenced drugs with the aim of identifying WPB size-reducing molecules that could be rapidly repurposed as antithrombotics. We found thirty-seven drugs with this activity, the majority of which can be grouped into pharmacological classes (**Table 1; Figure 2**). Some of these classes, such as microtubule depolymerizing agents and statins, have been identified by previous work [14, 15]. Others might be expected, due to their effects on the Golgi ribbon, as in the case of HDAC and Topoisomerase inhibitors [22, 23]. Our screen also identified compounds with pharmacology previously unknown to affect WPB biogenesis and size. Together, these findings suggest that several cellular pathways can modulate the size of WPBs produced by

endothelial cells.

Multidrug resistance protein 1 (MDR1) is an organic anion transporter. It's up-regulation is responsible for the development of tumor resistance to chemotherapy, hence its name. While this activity towards xenobiotics was the first to be identified, it has become clear that MRP1 is also involved in the cellular efflux of endogenous molecules, mediating pro-inflammatory signalling pathways and may act as an oxidative stress sensor [40]. Interestingly, more than a third of the novel WPB-shortening compounds with varied mechanisms of action (**Table 1; Figure 2; Table S2**) have also been described as MDR1 substrates and inhibitors. This suggests the possibility that, in addition to their main molecular target, these drugs could affect the efflux of endogenous MDR1 signalling substrates, which regulate WPB size through a mechanism to be elucidated by future investigations.

Since the screen endpoint was 24 h, the drugs we identified are relatively fast-acting. Several of the compounds display activity between sub-micromolar and low nanomolar concentrations (**Table 1**), which is likely to be compatible with their use in the clinic. The present study confirms statins' effects on WPB size remodelling [15]. Statins are known to rapidly produce anti-inflammatory and anticoagulant effects on the endothelium [41] and their acute administration in the context of percutaneous angioplasty greatly reduces post-operative myocardial infarctions [42]. The compounding of these fast-acting effects, WPB size-reduction included, suggests that statins may represent a promising tool for acute, emergency treatment in endotheliopathies involving inflammation, coagulation and thrombosis.

As a class, the most potent WPB-shortening drugs identified in this study, were the cardiac glycosides and their cardenolide precursors (**Figure 2B; Table 1**). Our testing of proscillaridin A, the most active among these compounds, shows that its WPB-shortening activity results in reduced plasma VWF recruitment to the endothelial surface, an *in vitro* antithrombotic phenotype (**Figure 4A**). It is worth noting that the proscillaridin concentration used in these assays is comparable to its plasma concentration in patients [43].

Considerations on drug toxicity. Our findings indicate that, with the caution due to their known dose-dependent cytotoxicity [44], cardiac glycosides may be worth exploring in acute and, perhaps, chronic antithrombotic therapies. Another novel WPB-shortening compound, cyclosporine A, was tested at a submaximal concentration with respect to its WPB-shortening activity. Despite the moderate effects on WPB size, cyclosporine at 1 μM caused a reduction in

plasma VWF recruitment to the endothelial surface in our *in vitro* antithrombotic assay (**Figure 4B-f**). As for proscillaridin, it is worth pointing out that this concentration is comparable to those that cyclosporine reaches in patient plasma after administration [45]. Proscillaridin and cyclosporine seem to act on WPB size through different mechanisms (**Figure 4C**). Our preliminary characterization suggests that proscillaridin reduces global protein synthesis, confirming a previous study on cardiac glycosides [25]. Interestingly, its effects on VWF levels are more pronounced than those on protein synthesis (**Figure 4A-d** and **4A-e**). This finding might indicate either some specificity of proscillaridin in reducing VWF synthesis or increasing its secretion or exerting an effect on its intracellular degradation, perhaps through WPB autophagy [46-48]. We rule out changes in VWF secretion, because in cells treated with another cardiac glycoside, lanatoside C (at 10 μM), while the cellular VWF levels were reduced, as a percentage of the total both its basal and histamine-stimulated release were identical to those of DMSO-treated controls (not shown); an indication that storage and secretion of VWF were not affected by this glycoside. Regardless the specific mechanism, our data suggest that at the concentration tested in our functional assays, proscillaridin is not cytotoxic, given that after 24 h incubation it did not reduce cell numbers, as opposed to two other compounds we tested at high concentration, clomipramine and astemizole (**Figure 4A** and **S1**). At the concentration tested, cyclosporine resulted in no changes of the parameters we measured except for a modest reduction in WPB size and its effects on plasma VWF adhesion (**Figure 4B**). Interestingly, calcineurin inhibition by cyclosporine results in activation of AMPK [49, 50]. Since AMPK is a positive regulator of GBF1 activity, which in turn reduces WPB size [16], cyclosporine indirect activation of this kinase could explain its effects on WPB size. Cyclosporine was also reported to stimulate UL-VWF secretion, which might explain the microangiopathic manifestations observed in a subset of organ transplant patients on anti-rejection therapy [51]. However, another study appears to contradict these conclusions, as specific inhibition of the calcineurin pool involved in WPB exocytosis results in decreased of VWF secretion [52]. While these reports suggest caution in the adoption of cyclosporine in antithrombotic therapies, our findings nevertheless warrant its investigation in this clinical context.

The compounds identified here are licenced and some have a decades-long history of clinical use. Their toxicity and therapeutic profiles are therefore well known. On the back of this knowledge, clinicians could design protocols for the safe testing of the most active WPB-shortening drugs in antithrombotic trials. In the context of potential drug toxicity, we would like to

note that combination of WPB-size reducing treatments, acting through different mechanisms, can display additive effects in the abatement of *in vitro* plasma VWF recruitment to the endothelial surface (**Figure S1D**). In a clinical setting, antithrombotic effects might therefore be achieved by administering combinations of drugs at submaximal concentrations with respect to their WPB-shortening activity.

Hypercoagulability in COVID-19. The disease caused by SARS-CoV-2 (COVID-19) displays a range of symptoms, the most immediately apparent being respiratory. However, testing of hospitalized patients has uncovered clinical manifestations, including haematological alterations, which correlate with poor prognosis. Some clinicians have described the hypercoagulability observed in critically ill patients as a form of disseminated intravascular coagulation (DIC) [53-59]. However, other retrospective studies and case reports have shown that these patients have unusually high levels of plasma VWF, suggesting that the hypercoagulability observed may be dependent on intravascular thrombosis [59-62].

We hope that the drug dataset reported here will provide clinicians and researchers with licensed candidates that may potentially progress to clinical trials for the treatment of the thrombotic complications of COVID-19. Apart from colchicine, which is being currently evaluated for COVID-19 therapy (https://clinicaltrials.gov/ct2/show/NCT04322682), we are not aware of other ongoing clinical trials in which the compounds we have identified are being tested. Our findings, however, prompt us to suggest that in the event of such trials, it might be important to also evaluate the haematological effects of the compounds under consideration.

In conclusion, the present study confirms the hypothesis that reduction in WPB size correlates with the diminished adhesive activity of its VWF cargo. The identification of several licenced compounds with fast-acting WPB-shortening activity, two of which we prove effective at concentrations compatible with their use in the clinic, paves the way to their repurposing for novel acute antithrombotic therapies involving organelle size modulation.

Methods

Cells. Human umbilical vein endothelial cells (HUVECs) were obtained commercially from PromoCell or Lonza. Cells were from pooled donors of both sexes expanded in our lab and used at

low passage (3 to 4), within 15 population doublings since isolation from umbilical cord. Cells were maintained in HGM (HUVEC Growth Medium) of the following composition: M199 (Gibco, Life Technologies), 20% Fetal Bovine Serum, (Labtech), 30 μg/mL endothelial cell growth supplement from bovine neural tissue and 10 U/mL Heparin (both from Sigma-Aldrich). Cells were cultured at 37 °C, 5% CO_2, in humidified incubators.

Reagents. The library compounds (1280 FDA-approved drugs), from Prestwick Chemical, were stored at –80 °C as 10 mM stock solutions in DMSO. For the initial screen, compounds were transferred to Echo Qualified 384-Well Low Dead Volume Microplates using the Echo® 520 acoustic dispenser (both from Labcyte). Concentration-response tests were carried out to confirm the activity of the primary hits and determine their WPB-shortening EC_{50} or lowest active concentration. In these experiments, each compound, starting at 10 μM, was diluted in two-fold steps across the eight wells of a 96-well plate columns (concentration range 78 nM - 10 μM), using the Echo® 520 acoustic dispenser as described above. Each compound was tested in duplicate plates for independent measurements. Antibodies used in this study were: rabbit polyclonal anti-VWF pro-peptide region [63], kindly provided by Dr. Carter (St. George's University, London); mouse monoclonal anti-GM130 (clone 35) from BD Biosciences; a rabbit polyclonal anti-VWF from DAKO (cat. no. A0082). DMSO (Hybri-Max™, cat. No. D2650), nocodazole (cat. No. M1404), proscillaridin A (cat. No. PHL82774), Cyclosporine A (cat. No. 30024) clomipramine (cat. No. C7291) and Astemizole (cat No. A2861) were from Sigma-Aldrich (now Merck Millipore). siRNA sequences targeting Luciferase and VWF were custom synthesised and previously described [15]. Normal pooled human plasma (Cryochek™; cat. No. CCN-15) was from Precision Biologic.

Drug screen. HUVECs were seeded on gelatin-coated 96-well plates (Nunclon surface©, NUNC) at 15000 cells/well and cultured. After 24 h, cells were rinsed with fresh medium and then library compounds were added with the Echo® 520 (Labcyte) acoustic dispenser and medium volume per well was adjusted with a MultiFlo FX dispenser (BioTek Instruments Inc.) to 100 μL for a final compound concentration of 10 μM. Plates were prepared in duplicate. Each plate contained one column treated with negative DMSO control (0.1%, final concentration) and one column treated

with Nocodazole positive control (3.3 μM, final concentration). All cells (DMSO-, Nocodazole- and compound-treated) received the same amount of DMSO vehicle (0.1% vol:vol). After 24 h treatment, cells were rinsed twice with warm, fresh HGM and fixed by incubation with 4% formaldehyde in PBS (10 min, RT).

Concentration-response experiments. HUVECs were seeded in 96-well plates and pre-processed as described for the screen. Hit compounds from
the primary screen were obtained by the Prestwick library and delivered to cells using the Echo® 520 acoustic dispenser (Labcyte) and cells were treated as described above. The concentrations of each compound ranged from 78 nM to 10 μM in 2-fold increments across the wells of one plate column. Duplicate plates were prepared. Each plate contained DMSO and Nocodozale controls as detailed for the screen. Treatment was for 24 h, at the end of which cells were fixed as described for the screen. Compounds were considered WPB-shortening drugs if, at least at the highest concentration tested (10 μM), their FA of long WPBs was ≤ 0.35. To determine the Proscillaridin A EC_{50}, a dedicated concentration-response experiment was carried out with two-fold dilutions along two columns of 96-well plates in duplicate (concentration range 76 pM - 2.5 μM).

Immunostaining and image acquisition. Fixed cells were processed for immunostaining as previously described [15]. WPBs were labelled using a rabbit polyclonal antibody to the VWF pro-peptide region. The Golgi apparatus was labeled with an anti-GM130 mAb. Primary antibodies were detected with Alexa Fluor dye-conjugated antibodies (Life Technologies). Nuclei were counterstained with 33342 (Life Technologies). Images (9 fields of view per well) were acquired with an Opera High Content Screening System (Perkin Elmer) using a 40x air objective (NA 0.6). For small-scale HTM experiments, imaging was carried out with similar parameters using either the Opera or the Opera Phenix High Content Screening Systems (Perkin Elmer).

High-throughput morphometry (HTM) workflow. Image processing and extraction of morphological parameters (high-throughput morphometry, HTM) have been described in detail elsewhere [14]. *R* scripts for image for data processing are available upon request. WPB size was expressed per well (i.e., summing the values measured in the 9 fields of view acquired per well) as the fraction of the total WPB area covered by WPBs > 2 μm. This morphometric approach was used also to measure WPB numbers and cell numbers (nuclei). WPB size was expressed per well

(i.e., summing the values measured in the 9 fields of view acquired per well) as the fraction of the total WPB area covered by WPBs > 2 μm. This morphometric approach was used also to measure WPB numbers and cell numbers (nuclei). Normalization and scoring were done using the cellHTS2 (version 2.46.1) Bioconductor *R* package [64]. DMSO negative controls were used for per plate median percent of control (POC) normalization. The *k*th compound value *x* in *i*th plate and replicate x_{ki} is relative to the average of within-plate negative controls.

$$x_{ki}^{POC} = \frac{x_{ki}}{\mu_i^{neg}} * 100$$

where μ_i^{neg} is the average of the measurements on the negative controls in the *i*th plate and replicate. Normalized values were scored using robust z-score method by subtracting the overall median from each measurement and dividing the result by the overall median absolute deviation. *R* scripts for data processing are available upon request. Concentration-response data analysis was done in *R* language, using the DRC package by Christian Ritz and Jens C. Strebig (https://CRAN.R-project.org/package=drc). The drm() function was used to fit a dose-response model, a four-parameter log-logistic function (LL.4), applied to each dataset; four parameter values were calculated: slope, lower limit, upper limit and EC_{50} value.

VWF and protein assays. For protein and VWF determinations, cells were cultured in 12-well plates and subjected to drug treatments as described for HTM experiments. Cells were then rinsed twice with PBS and lysed with ice-cold cold RIPA buffer (100 mM Tris-HCl, pH 7.5, 150 mM NaCl, 1% TX-100, 0.5% Na-Deoxycholate and 0.05% SDS) supplemented with protease inhibitor cocktail (P8340, Sigma-Aldrich) and clarified by centrifugation. VWF cell content was measured by a sandwich ELISA as previously detailed [15]. VWF amounts were calculated by converting the volumes of the pooled plasma used for standard curves into nanograms of vWF (1 μL human pooled plasma = 10 ng VWF). Protein content in HUVEC lysates was measured using the Pierce™ BCA Protein Assay Kit (Cat. No. 23225). Two biological replicates, each with 3 technical replicates were analysed in these experiments.

Plasma VWF recruitment assays. HUVECs were seeded in HGM on gelatin-coated Ibidi VI μ-slides (Thistle Scientific). At 24 h, cells were rinsed with three changes of fresh medium and drug treatment was started. After 24 h, μ-slides were attached to a pump system (Harvard Apparatus, Holliston, MA, USA), while kept in a heated chamber (37 °C) for the duration of the assay. Cells

were initially perfused with Ca^{2+}/Mg^{2+} Hanks' balanced salt solution (HBBS; Life Technologies, Cat no. 14025092) supplemented with 0.2% BSA for 2 minutes. Cells were then perfused with HBBS containing 100 µM histamine for a further 3 minutes in order to stimulate VWF exocytosis, followed by perfusion for 1 minute with human pooled plasma supplemented with histamine (Cryochek ™; Precision Biologic, cat. no. CCN-15). A constant flow rate was kept throughout the perfusion and produced a wall shear stress of 2.5 dynes/cm^2 (0.25 MPa). Finally, cells were fixed by perfusion of 4% formaldehyde in PBS: 2 minutes at 2.5 dynes/cm^2, followed 2 min at 1.25 dynes/cm^2. Flow was then stopped and cells kept in fixative solution in static condition for 6 more minutes. Fixed cells were then rinsed with PBS. *Immunostaining and confocal microscopy*. After blocking treatment with 5% (BSA) in PBS for 30 minutes, non-permeabilized samples were incubated with a polyclonal anti-VWF antibody (DAKO, cat. No. A00A2; 1:1000 in 1% BSA/PBS) for 1 hour, in order to label cell surface-associated VWF. Samples were then incubated with an anti-rabbit Alexa Fluor564-conjugated antibody and Hoechst 33342 (both from Life Technologies) at 1:500 and 1:10000, respectively, in 1% BSA/PBS for 45 minutes. Images were acquired at a spinning disc confocal microscope (UltraView VoX, Perkin Elmer) with a 20x objective. For each treatment, a tiled image panel (36 fields of view in a 3x12 grid) with a number of z-slices sufficient to visualise the entire depth of the sample was acquired. Quantification of surface VWF was done with Fiji (ImageJ). Each field of view was assessed independently. Z-stacks were converted into maximum intensity projections. VWF fluorescence signals were thresholded and converted into binary values. For each field of view, the area covered by the VWF signal was measured using ImageJ's 'Analyse particle' function. Experiments involving VWF level reduction by siRNA and statin treatment were carried out with as previously described [15]. Each treatment was replicated with similar results in at least two independent experiments.

Compound	**EC_{50} ± S.E. or lowest active concentrations (µM)**	**Compound**	**EC_{50} ± S.E. or lowest active concentrations (µM)**
Monensin (1)	≤ 78 nM	**Itraconazole (9, 18)**	1.891 ± 0.407
Colchicine (2, 18)	≤ 78 nM	**Digoxigenin (3, 5)**	2.172 ± 0.804
Podophyllotoxin (2)	≤ 78 nM	**Hexachlorophene (10)**	2.376 ± 0.439
Proscillaridin A (3, 5)	0.018 ± 0.003	**Mitoxantrone (6)**	2.958 ± 0.356
Fluvastatin (4, 11)	0.198 ± 0.070	**Parbendazole (2)**	4.402 ± 0.986
Digoxin (3, 5, 18)	0.254 ± 0.047	**Vorinostat (11)**	4.622 ± 0.867

Lanatoside C (3, 5)	0.515 ± 0.203	**Clomipramine (12, 13, 18)**	4.699 ± 1.191
Cycloheximide (5)	0.532 ± 0.104	**Verteporfin ***	5 μM
Simvastatin (4, 11, 18)	0.557 ± 0.195	**Tegaserod (13)**	10 μM
Daunorubicin (6, 18)	0.662 ± 0.139	**Bepridil (3, 14, 18)**	10 μM
Doxorubicin (6, 18)	0.678 ± 0.246	**Maprotiline (12, 15)**	10 μM
Digitoxigenin (3, 5)	0.839 ± 0.062	**Camptothecine (6)**	10 μM
Atorvastatin (4, 11, 18)	0.951 ± 0.312	**Clomiphene (10)**	10 μM
Nocodazole (2)	1.046 ± 0.266	**Astemizole (15, 18)**	10 μM
Cyclosporin A (7, 18)	1.071 ± 0.186	**Thonzonium (1)**	10 μM
Aprepitant (8)	1.230 ± 0.153	**Alclometasone (16)**	10 μM
Pyrvinium *	1.256 ± 0.143	**Quinacrine (17, 18)**	10 μM
Lovastatin (4, 11, 18)	1.441 ± 0.261	**Ciclesonide (16)**	10 μM
Mevastatin (4)	1.768 ± 0.213		

Table 1. WPB-shortening compounds identified and confirmed in concentration-response experiments in the range 0.078 - 10 μM. The EC_{50} (± standard error) or the lowest concentrations showing WPB-shortening activity for each compound, within this concentration range, are indicated. For proscillaridin A, a cardiac glycoside, a second set of experiments was carried out to determine its EC_{50}. The pharmacology (primary and other known targets) of each compound is indicated by the numbers within parentheses: 1, Trans-membrane pH gradient depleting agents; 2, Microtubule polymerization inhibitors; 3, Na/K-ATPase inhibitors; 4, HMGCR inhibitors/Statins; 5, Protein synthesis inhibitors; 6, DNA interaclating agents/Topoisomerase inhibitors; 7, Protein phosphatase inhibitors; 8, Neurokinin receptor antagonists; 9, Ergosterol synthesis inhibitors; 10, Estrogen receptor agonists; 11, HDAC inhibitors; 12, Noradrenaline reuptake inhibitors; 13, Serotonin Receptor antagonists and serotonin reuptake inhibitors; 14, Voltage-dependent Ca2+ inhibitors; 15, Histamine receptor antagonists; 16, Glucocorticord receptor agonist; 17, PLA2 inhibitors; 18, MDR1/ABCB1 inhibitors . *, pyrvinium and verteporfin have no known molecular targets.

Figure Legends

Figure 1. Drug screen: design, execution and results. A. WPB sizes range between 0.5 and 5 μm. To measure a single quantitative parameter accounting for WPB size in a organelle population, we calculated the "fraction of the area (FA) covered by long (i.e., > 2 μm) WPBs. **B**.

DMSO and Nocodazole were used as negative and positive control treatments, respectively, for reducing WPB size. Micrographs show the effects of the two control treatments on HUVECs (24 h); scale bar: 20 μm (inset, 10 μm). **C**. Quantification of the "FA of long WPBs" for cells treated as in B. Data-points represent the values calculated for each well of a 96-well plate; median and interquartile ranges are shown. ****, $P < 0.0001$; Mann-Whitney test. **D**. Screen setup. Individual library drugs were dispensed into single wells of 96-well plates, which also had two columns treated with DMSO and Nocodazole controls. Two plates with identical drug layout (biological duplicates) were analyzed. **E**. Screen results. Z-scores of the library drugs are plotted. Hit drugs were selected based on the effects of fluvastatin and simvastatin, which we previously showed to reduce WPB size. Fluvastatin, with the lowest Z-score, was used as cut-off for the selection of hit compounds. **F**. Concentration-response experiments were carried out on the initial screen hits, by two-fold dilutions (starting at 10 μM) along 96-well plate columns with each compound tested in duplicate plates. FA of long WPBs was measured for each drug concentration allowing calculation of their EC_{50} or identification of their lowest effective concentration in the range tested.

Figure 2. Classification of WPB-shortening drugs. A survey of the mechanisms of action (see Table S2) identified molecular targets for thirty-five of the thirty-seven compounds with WPB-shortening activity. **A**. Based on the information retrieved, targets were classifies as "primary" or "other" and represented in a tabular form in order to show the "cross-talk" between pharmacological classes. **B**. Pharmacological classes with at least two compounds were graphically represented and ranked by "potency" using the median value (black bars) of their EC_{50} or lowest active concentration (the data points in the plots) identified in this work. The lowest value (78 nM) was considered for those drugs found active at all concentrations tested in this work except for proscillaridin A, whose EC_{50} (18 nM) was measured in a dedicated set of experiments. Numbering in parentheses is as in Table 1.

Figure 3. **Cardiac glycosides and cardenolides**. **A**. Original micrographs from the screen of HUVECs treated for 24 h with 10 μM each of the indicated compounds. Treatment with these molecules induces WPB-shortening and Golgi apparatus compaction (compare to DMSO negative control). Scale bar: 10 μm. **B**. Concentration-response curves of cardiac glycoside and cardenolide activity on WPB size; calculated EC_{50} values are reported.

Figure 4. Antithrombotic effect of novel WPB-size reducing compounds. WPB size and numbers, cell numbers, protein and VWF content (**a-e**) of HUVECs treated with the cardiac glycoside proscilladirin (**A**) and the protein phosphatase inhibitor cyclosporine (**B**) at the concentration tested in VWF plasma recruitment assays (**f**). Data points in **a**, **b** and **c** panels are from experiments done in 96-well plates, with one column per treatment. Data points in panels **d** and **e** are samples in 12-well plates (one data point per well). Data points in panels **f** are from 36 fields of view per treatment. Individual data points with median and interquartile ranges are shown. **, *** and ****: $P < 0.01$, 0.001 and 0.0001, respectively (Mann-Whitney test). **C**. Tabular summary of the experiments in **A** and **B**.

Figure S1. Additional data. A and **B.** In concentration-response experiments, clomipramine and astemizole were effective in shortening WPB size at 10 μM (see Table 1, main text). To test whether higher concentrations of these compounds would induce a stronger effect, titration experiments were carried out. Both compounds did cause stronger organelle shortening at 20 and 50 μM. However, these effects resulted from cytotoxicity, as shown by cell depletion from the wells. Clomipramine was toxic at concentrations > 20 μM, while astemizole was toxic above 10 μM. Experiments were carried out as detailed in the legend of Figure 4. *, ** and ***: $P < 0.05$, 0.01 and 0.001, respectively (Mann-Whitney test). **C**. Concentration-response curve of Cyclosporine A. **D**. Additive effects of the combination of two WPB-size reducing treatments. WPB size was reduced by decreasing cellular VWF level or by statin incubation or their combination. ****, $P < 0.0001$. Mann-Whitney test. Black asterisks label comparisons with Luciferase-siRNA/DMSO control. Red asterisks labels caparisons of both VWF-siRNA/DMSO and Luciferase-siRNA/Simvastatin with VWF-siRNA/Simvastatin.

Author contributions. F.F., F.P., R.K. and D.F.C designed the study. F.F., F.P. and J.C. did experiments. J.K.-V., F.P. and F.F. analysed data. R.K. provided fundamental reagents and instrumentation. F.F and D.F.C. wrote the manuscript.

Acknowledgements. The authors wish to thank John Greenwood, Marie Ann Scully, Laura Benjamin and Martin Raff for their valuable comments on the manuscript.

F. F., F.P. and D.F.C. were funded by the MRC grant MC_UU_12018/2 awarded to DFC. R.K. J.C, and J. K.-V. were funded by the MRC grant MC_U12266B.

Conflict of Interest Disclosure. The authors have no conflicts of interest to declare.

References

1 Sadler JE. Biochemistry and genetics of von Willebrand factor. *Annu Rev Biochem*. 1998; **67**: 395-424. 10.1146/annurev.biochem.67.1.395.

2 Ruggeri ZM, Mendolicchio GL. Interaction of von Willebrand factor with platelets and the vessel wall. *Hamostaseologie*. 2015; **35**. 10.5482/HAMO-14-12-0081.

3 Zhang X, Halvorsen K, Zhang CZ, Wong WP, Springer TA. Mechanoenzymatic cleavage of the ultralarge vascular protein von Willebrand factor. *Science (New York, NY*. 2009; **324**: 1330-4.

4 Chang JC. Sepsis and septic shock: endothelial molecular pathogenesis associated with vascular microthrombotic disease. *Thromb J*. 2019; **17**: 10. 10.1186/s12959-019-0198-4.

5 Tsai HM. Pathophysiology of thrombotic thrombocytopenic purpura. *Int J Hematol*. 2010; **91**: 1-19. 10.1007/s12185-009-0476-1.

6 Apostolova MH, Seaman CD, Comer DM, Yabes JG, Ragni MV. Prevalence and Risk Factors Associated With Hypertension in von Willebrand Disease. *Clin Appl Thromb Hemost*. 2018; **24**: 93-9. 10.1177/1076029616670258.

7 Westein E, Hoefer T, Calkin AC. Thrombosis in diabetes: a shear flow effect? *Clin Sci (Lond)*. 2017; **131**: 1245-60. 10.1042/CS20160391.

8 Kanaji S, Fahs SA, Shi Q, Haberichter SL, Montgomery RR. Contribution of platelet vs. endothelial VWF to platelet adhesion and hemostasis. *J Thromb Haemost*. 2012; **10**: 1646-52. 10.1111/j.1538-7836.2012.04797.x.

9 Nichols TC, Samama CM, Bellinger DA, Roussi J, Reddick RL, Bonneau M, Read MS, Bailliart O, Koch GG, Vaiman M, et al. Function of von Willebrand factor after crossed bone marrow transplantation between normal and von Willebrand disease pigs: effect on arterial thrombosis in chimeras. *Proceedings of the National Academy of Sciences of the United States of America*. 1995; **92**: 2455-9.

10 McCormack JJ, Lopes da Silva M, Ferraro F, Patella F, Cutler DF. Weibel-Palade bodies at a glance. *Journal of cell science*. 2017; **130**: 3611-7. 10.1242/jcs.208033.

11 Arya M, Anvari B, Romo GM, Cruz MA, Dong JF, McIntire LV, Moake JL, Lopez JA. Ultralarge multimers of von Willebrand factor form spontaneous high-strength bonds with the platelet glycoprotein Ib-IX complex: studies using optical tweezers. *Blood*. 2002; **99**: 3971-7. 10.1182/blood-2001-11-0060.

12 Rybaltowski M, Suzuki Y, Mogami H, Chlebinska I, Brzoska T, Tanaka A, Banno F, Miyata T, Urano T. In vivo imaging analysis of the interaction between unusually large von Willebrand factor multimers and platelets on the surface of vascular wall. *Pflugers Arch*. 2011; **461**: 623-33. 10.1007/s00424-011-0958-x.

13 Nicolay JP, Thorn V, Daniel C, Amann K, Siraskar B, Lang F, Hillgruber C, Goerge T, Hoffmann S, Gorzelanny C, Huck V, Mess C, Obser T, Schneppenheim R, Fleming I, Schneider MF, Schneider SW. Cellular stress induces erythrocyte assembly on intravascular von Willebrand factor strings and promotes microangiopathy. *Sci Rep*. 2018; **8**: 10945. 10.1038/s41598-018-28961-2.

14 Ferraro F, Kriston-Vizi J, Metcalf DJ, Martin-Martin B, Freeman J, Burden JJ, Westmoreland D, Dyer CE, Knight AE, Ketteler R, Cutler DF. A two-tier Golgi-based control of organelle size underpins the functional plasticity of endothelial cells. *Developmental cell*. 2014; **29**: 292-304. 10.1016/j.devcel.2014.03.021.

15 Ferraro F, Lopes da Silva M, Grimes W, Lee HK, Ketteler R, Kriston-Vizi J, Cutler DF. Weibel-Palade body size modulates the adhesive activity of its von Willebrand Factor cargo in cultured endothelial cells. *Sci Rep*. 2016; **6**: 32473. 10.1038/srep32473.

16 Lopes-da-Silva M, McCormack JJ, Burden JJ, Harrison-Lavoie KJ, Ferraro F, Cutler DF. A GBF1-Dependent Mechanism for Environmentally Responsive Regulation of ER-Golgi Transport. *Developmental cell*. 2019; **49**: 786-801 e6. 10.1016/j.devcel.2019.04.006.

17 van Agtmaal EL, Bierings R, Dragt BS, Leyen TA, Fernandez-Borja M, Horrevoets AJ, Voorberg J. The shear stress-induced transcription factor KLF2 affects dynamics and angiopoietin-2 content of Weibel-Palade bodies. *PLoS One*. 2012; **7**: e38399. 10.1371/journal.pone.0038399.

18 Ketteler R, Freeman J, Ferraro F, Bata N, Cutler DF, Kriston-Vizi J, Stevenson N. Image-based siRNA screen to identify kinases regulating Weibel-Palade body size control using electroporation. *Scientific data*. 2017; **4**: 170022. 10.1038/sdata.2017.22.

19 Stevenson NL, Martin-Martin B, Freeman J, Kriston-Vizi J, Ketteler R, Cutler DF. G protein-coupled receptor kinase 2 moderates recruitment of THP-1 cells to the endothelium by limiting histamine-invoked Weibel-Palade body exocytosis. *J Thromb Haemost*. 2014; **12**: 261-72. 10.1111/jth.12470.

20 McCormack JJ, Harrison-Lavoie KJ, Cutler DF. Human endothelial cells size-select their secretory granules for exocytosis to modulate their functional output. *J Thromb Haemost*. 2020; **18**: 243-54. 10.1111/jth.14634.

21 Thyberg J, Moskalewski S. Microtubules and the organization of the Golgi complex. *Exp Cell Res*. 1985; **159**: 1-16.

22 Gendarme M, Baumann J, Ignashkova TI, Lindemann RK, Reiling JH. Image-based drug screen identifies HDAC inhibitors as novel Golgi disruptors synergizing with JQ1. *Molecular biology of the cell*. 2017; **28**: 3756-72. 10.1091/mbc.E17-03-0176.

23 Farber-Katz SE, Dippold HC, Buschman MD, Peterman MC, Xing M, Noakes CJ, Tat J, Ng MM, Rahajeng J, Cowan DM, Fuchs GJ, Zhou H, Field SJ. DNA damage triggers Golgi dispersal via DNA-PK and GOLPH3. *Cell*. 2014; **156**: 413-27. 10.1016/j.cell.2013.12.023.

24 Michaux G, Abbitt KB, Collinson LM, Haberichter SL, Norman KE, Cutler DF. The physiological function of von Willebrand's factor depends on its tubular storage in endothelial Weibel-Palade bodies. *Developmental cell*. 2006; **10**: 223-32.

25 Perne A, Muellner MK, Steinrueck M, Craig-Mueller N, Mayerhofer J, Schwarzinger I, Sloane M, Uras IZ, Hoermann G, Nijman SM, Mayerhofer M. Cardiac glycosides induce cell death in human cells by inhibiting general protein synthesis. *PLoS One*. 2009; **4**: e8292. 10.1371/journal.pone.0008292.

26 Newman RA, Yang P, Pawlus AD, Block KI. Cardiac glycosides as novel cancer therapeutic agents. *Mol Interv*. 2008; **8**: 36-49. 10.1124/mi.8.1.8.

27 Triana-Martinez F, Picallos-Rabina P, Da Silva-Alvarez S, Pietrocola F, Llanos S, Rodilla V, Soprano E, Pedrosa P, Ferreiros A, Barradas M, Hernandez-Gonzalez F, Lalinde M, Prats N, Bernado C, Gonzalez P, Gomez M, Ikonomopoulou MP, Fernandez-Marcos PJ, Garcia-Caballero T, Del Pino P, Arribas J, Vidal A, Gonzalez-Barcia M, Serrano M, Loza MI, Dominguez E, Collado M. Identification and characterization of Cardiac Glycosides as senolytic compounds. *Nature communications*. 2019; **10**: 4731. 10.1038/s41467-019-12888-x.

28 Jorgensen KA, Koefoed-Nielsen PB, Karamperis N. Calcineurin phosphatase activity and immunosuppression. A review on the role of calcineurin phosphatase activity and the immunosuppressive effect of cyclosporin A and tacrolimus. *Scand J Immunol*. 2003; **57**: 93-8. 10.1046/j.1365-3083.2003.01221.x.

29 Ruggeri ZM. The role of von Willebrand factor in thrombus formation. *Thromb Res*. 2007; **120 Suppl 1**: S5-9. 10.1016/j.thromres.2007.03.011.

30 Varga-Szabo DP, I.; Nieswandt, B.;. Cell adhesion mechanisms in platelets. *Arteriosclerosis, Thrombosis and Vascular Biology*. 2008; **28**: 403-12. 10.1161/ATVBAHA.107.150474.

31 Pappelbaum KI, Gorzelanny C, Grassle S, Suckau J, Laschke MW, Bischoff M, Bauer C, Schorpp-Kistner M, Weidenmaier C, Schneppenheim R, Obser T, Sinha B, Schneider SW.

Ultralarge von Willebrand factor fibers mediate luminal Staphylococcus aureus adhesion to an intact endothelial cell layer under shear stress. *Circulation*. 2013; **128**: 50-9. 10.1161/CIRCULATIONAHA.113.002008.

32 Bauer AT, Suckau J, Frank K, Desch A, Goertz L, Wagner AH, Hecker M, Goerge T, Umansky L, Beckhove P, Utikal J, Gorzelanny C, Diaz-Valdes N, Umansky V, Schneider SW. von Willebrand factor fibers promote cancer-associated platelet aggregation in malignant melanoma of mice and humans. *Blood*. 2015; **125**: 3153-63. 10.1182/blood-2014-08-595686.

33 Marshall WF. Organelle size control systems: from cell geometry to organelle-directed medicine. *Bioessays*. 2012; **34**: 721-4. 10.1002/bies.201200043.

34 Fledderus JO, van Thienen JV, Boon RA, Dekker RJ, Rohlena J, Volger OL, Bijnens AP, Daemen MJ, Kuiper J, van Berkel TJ, Pannekoek H, Horrevoets AJ. Prolonged shear stress and KLF2 suppress constitutive proinflammatory transcription through inhibition of ATF2. *Blood*. 2007; **109**: 4249-57. 10.1182/blood-2006-07-036020.

35 Dekker RJ, Boon RA, Rondaij MG, Kragt A, Volger OL, Elderkamp YW, Meijers JC, Voorberg J, Pannekoek H, Horrevoets AJ. KLF2 provokes a gene expression pattern that establishes functional quiescent differentiation of the endothelium. *Blood*. 2006; **107**: 4354-63. 10.1182/blood-2005-08-3465.

36 Kumar A, Lin Z, SenBanerjee S, Jain MK. Tumor necrosis factor alpha-mediated reduction of KLF2 is due to inhibition of MEF2 by NF-kappaB and histone deacetylases. *Mol Cell Biol*. 2005; **25**: 5893-903. 10.1128/MCB.25.14.5893-5903.2005.

37 Lin Z, Kumar A, SenBanerjee S, Staniszewski K, Parmar K, Vaughan DE, Gimbrone MA, Jr., Balasubramanian V, Garcia-Cardena G, Jain MK. Kruppel-like factor 2 (KLF2) regulates endothelial thrombotic function. *Circ Res*. 2005; **96**: e48-57. 10.1161/01.RES.0000159707.05637.a1.

38 Parmar KM, Nambudiri V, Dai G, Larman HB, Gimbrone MA, Jr., Garcia-Cardena G. Statins exert endothelial atheroprotective effects via the KLF2 transcription factor. *The Journal of biological chemistry*. 2005; **280**: 26714-9. 10.1074/jbc.C500144200.

39 Sen-Banerjee S, Mir S, Lin Z, Hamik A, Atkins GB, Das H, Banerjee P, Kumar A, Jain MK. Kruppel-like factor 2 as a novel mediator of statin effects in endothelial cells. *Circulation*. 2005; **112**: 720-6. 10.1161/CIRCULATIONAHA.104.525774.

40 Cole SP. Multidrug resistance protein 1 (MRP1, ABCC1), a "multitasking" ATP-binding cassette (ABC) transporter. *The Journal of biological chemistry*. 2014; **289**: 30880-8. 10.1074/jbc.R114.609248.

41 Greenwood J, Mason JC. Statins and the vascular endothelial inflammatory response. *Trends Immunol*. 2007; **28**: 88-98. 10.1016/j.it.2006.12.003.

42 Leoncini M, Toso A, Maioli M, Tropeano F, Bellandi F. Statin treatment before percutaneous cononary intervention. *Journal of thoracic disease*. 2013; **5**: 335-42. 10.3978/j.issn.2072-1439.2013.05.09.

43 Andersson K-E, Bergdahl B, Bodem G, Dengler HJ, Dutta S, Foster JM, Greeff K, Grosse-Brockhoff F, Krieglstein J, Lauterbach F, Lee G, Manninen V, Mason DT, Nyberg L, Ochs HR, Peters U, Rietbrock N, Shaw TRD, Stewart GA, Storstein L, Wirth KE, Woodcock BG. *Cardiac Glycosides Part II: Pharmacokinetics and Clinical Pharmacology*. Berlin Heidelberg New York: Springer-Verlag, 1981.

44 Kanji S, MacLean RD. Cardiac glycoside toxicity: more than 200 years and counting. *Crit Care Clin*. 2012; **28**: 527-35. 10.1016/j.ccc.2012.07.005.

45 Legg B, Gupta SK, Rowland M, Johnson RW, Solomon LR. Cyclosporin: pharmacokinetics and detailed studies of plasma and erythrocyte binding during intravenous and oral administration. *Eur J Clin Pharmacol*. 1988; **34**: 451-60. 10.1007/BF01046701.

46 Wang Y, Qiu Q, Shen JJ, Li DD, Jiang XJ, Si SY, Shao RG, Wang Z. Cardiac glycosides induce autophagy in human non-small cell lung cancer cells through regulation of dual signaling pathways. *Int J Biochem Cell Biol*. 2012; **44**: 1813-24. 10.1016/j.biocel.2012.06.028.

47 Torisu T, Torisu K, Lee IH, Liu J, Malide D, Combs CA, Wu XS, Rovira, II, Fergusson MM, Weigert R, Connelly PS, Daniels MP, Komatsu M, Cao L, Finkel T. Autophagy regulates endothelial cell processing, maturation and secretion of von Willebrand factor. *Nat Med*. 2013; **19**: 1281-7. 10.1038/nm.3288.

48 Hundeshagen P, Hamacher-Brady A, Eils R, Brady NR. Concurrent detection of autolysosome formation and lysosomal degradation by flow cytometry in a high-content screen for inducers of autophagy. *BMC biology*. 2011; **9**: 38. 10.1186/1741-7007-9-38.

49 Park HG, Yi H, Kim SH, Yu HS, Ahn YM, Lee YH, Roh MS, Kim YS. The effect of cyclosporine A on the phosphorylation of the AMPK pathway in the rat hippocampus. *Prog Neuropsychopharmacol Biol Psychiatry*. 2011; **35**: 1933-7. 10.1016/j.pnpbp.2011.09.008.

50 Lee CR, Chun JN, Kim SY, Park S, Kim SH, Park EJ, Kim IS, Cho NH, Kim IG, So I, Kim TW, Jeon JH. Cyclosporin A suppresses prostate cancer cell growth through CaMKKbeta/AMPK-mediated inhibition of mTORC1 signaling. *Biochem Pharmacol*. 2012; **84**: 425-31. 10.1016/j.bcp.2012.05.009.

51 Nolasco LH, Gushiken FC, Turner NA, Khatlani TS, Pradhan S, Dong JF, Moake JL, Vijayan KV. Protein phosphatase 2B inhibition promotes the secretion of von Willebrand factor from endothelial cells. *J Thromb Haemost*. 2009; **7**: 1009-18. 10.1111/j.1538-7836.2009.03355.x.

52 Da Q, Shaw T, Pradhan S, Roche PA, Cruz MA, Vijayan KV. Disruption of protein complexes containing protein phosphatase 2B and Munc18c reduces the secretion of von Willebrand factor from endothelial cells. *J Thromb Haemost*. 2017; **15**: 1032-9. 10.1111/jth.13671.

53 Cui S, Chen S, Li X, Liu S, Wang F. Prevalence of venous thromboembolism in patients with severe novel coronavirus pneumonia. *J Thromb Haemost*. 2020. 10.1111/jth.14830.

54 Zhang Y, Xiao M, Zhang S, Xia P, Cao W, Jiang W, Chen H, Ding X, Zhao H, Zhang H, Wang C, Zhao J, Sun X, Tian R, Wu W, Wu D, Ma J, Chen Y, Zhang D, Xie J, Yan X, Zhou X, Liu Z, Wang J, Du B, Qin Y, Gao P, Qin X, Xu Y, Zhang W, Li T, Zhang F, Zhao Y, Li Y, Zhang S. Coagulopathy and Antiphospholipid Antibodies in Patients with Covid-19. *N Engl J Med*. 2020. 10.1056/NEJMc2007575.

55 Wang J, Hajizadeh N, Moore EE, McIntyre RC, Moore PK, Veress LA, Yaffe MB, Moore HB, Barrett CD. Tissue Plasminogen Activator (tPA) Treatment for COVID-19 Associated Acute Respiratory Distress Syndrome (ARDS): A Case Series. *J Thromb Haemost*. 2020. 10.1111/jth.14828.

56 Lillicrap D. Disseminated intravascular coagulation in patients with 2019-nCoV pneumonia. *J Thromb Haemost*. 2020; **18**: 786-7. 10.1111/jth.14781.

57 Tang N, Li D, Wang X, Sun Z. Abnormal coagulation parameters are associated with poor prognosis in patients with novel coronavirus pneumonia. *J Thromb Haemost*. 2020; **18**: 844-7. 10.1111/jth.14768.

58 Terpos E, Ntanasis-Stathopoulos I, Elalamy I, Kastritis E, Sergentanis TN, Politou M, Psaltopoulou T, Gerotziafas G, Dimopoulos MA. Hematological findings and complications of COVID-19. *Am J Hematol*. 2020. 10.1002/ajh.25829.

59 Marietta M, Ageno W, Artoni A, De Candia E, Gresele P, Marchetti M, Marcucci R, Tripodi A. COVID-19 and haemostasis: a position paper from Italian Society on Thrombosis and Haemostasis (SISET). *Blood Transfus*. 2020. 10.2450/2020.0083-20.

60 Escher R, Breakey N, Lammle B. Severe COVID-19 infection associated with endothelial activation. *Thromb Res*. 2020; **190**: 62. 10.1016/j.thromres.2020.04.014.

61 Helms J, Tacquard C, Severac F, Leonard-Lorant I, Ohana M, Delabranche X, Merdji H, Clere-Jehl R, Schenck M, Fagot Gandet F, Fafi-Kremer S, Castelain V, Schneider F, Grunebaum L, Angles-Cano E, Sattler L, Mertes PM, Meziani F, Group CT. High risk of thrombosis in

patients with severe SARS-CoV-2 infection: a multicenter prospective cohort study. *Intensive Care Med*. 2020; **46**: 1089-98. 10.1007/s00134-020-06062-x.

62 Goshua G, Pine AB, Meizlish ML, Chang CH, Zhang H, Bahel P, Baluha A, Bar N, Bona RD, Burns AJ, Dela Cruz CS, Dumont A, Halene S, Hwa J, Koff J, Menninger H, Neparidze N, Price C, Siner JM, Tormey C, Rinder HM, Chun HJ, Lee AI. Endotheliopathy in COVID-19-associated coagulopathy: evidence from a single-centre, cross-sectional study. *Lancet Haematol*. 2020. 10.1016/S2352-3026(20)30216-7.

63 Hewlett L, Zupancic G, Mashanov G, Knipe L, Ogden D, Hannah MJ, Carter T. Temperature-dependence of Weibel-Palade body exocytosis and cell surface dispersal of von Willebrand factor and its propolypeptide. *PLoS One*. 2011; **6**: e27314. 10.1371/journal.pone.0027314.

64 Boutros M, Bras LP, Huber W. Analysis of cell-based RNAi screens. *Genome biology*. 2006; **7**: R66. 10.1186/gb-2006-7-7-R66.

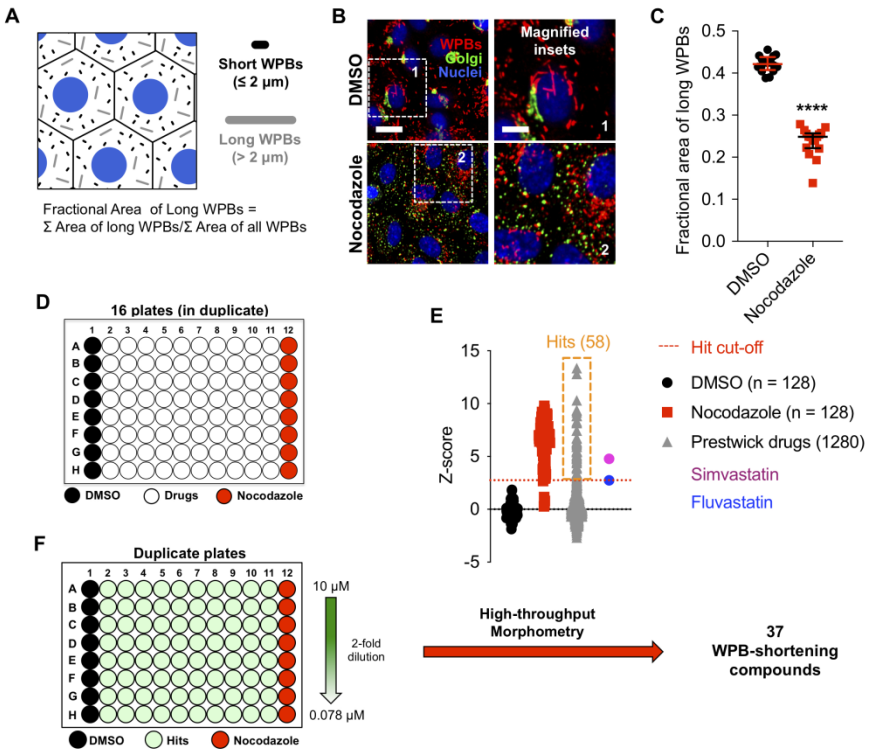

Figure 1

jth_15084_f1.tiff

Figure 2

A

	Primary targets	Other targets				
		MDR1 inh	Prot inh	HDAC inh	5HTR ant/5HT-RU inh	HR ant
Na/K inh	5	1	5			
HMGCR inh	5	3		4		
MT inh	4	1				
TIase inh	4	2				
pH depl	2					
ER ant	2					
GR ago	2					
NARI	2	1			1	1
5HTR ant	1				1	
NKR ant	1					
Ca Ch inh	1	1				
Prot inh	1					
PPase inh	1	1				
HDAC inh	1					
Ergo inh	1	1				
HR ant	1	1				1
PLA2 inh	1	1				
Total	35	13	5	4	2	2

B

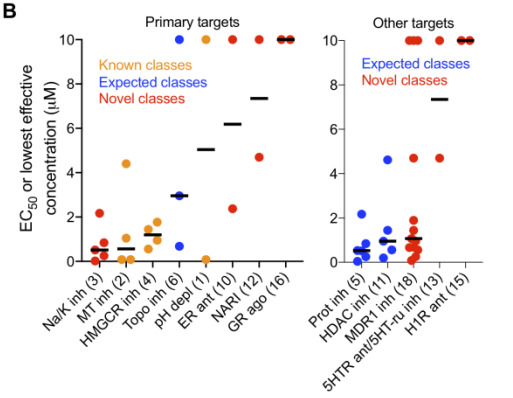

Abbreviations
MT inh: microtubule inhibitor
Na/K inh: Na^+/K^+-ATPase inhibitors (**cardiac glycosides** and **cardenolides**)
HMGCR inh: 3-hydroxy, 3-methylglutaryl-CoA reductase inhibitors (**statins**)
Topo inh: Topoisomerase inhibitors
pH depl: transmembrane pH gradient depleting agents
ER ant: estrogen receptor antagonists
NARI: noradrenaline reuptake inhibitors
GR ago: glucocorticoid receptor agonists
Prot inh: protetin synthesis inhibitors
HDAC inh: histone deacetylase inhibitors
MDR1 inh: multidrug resistance protein 1 (ABCB1) inhibitors
5HTR ant: 5-hydroxythryptamine (serotonin) receptor antagonists
5HT-RI inh: 5-hydroxythryptamine (serotonin) reuptake inhibitors
H1R ant: histamine 1 receptor antagonists

jth_15084_f2.tiff

Figure 3

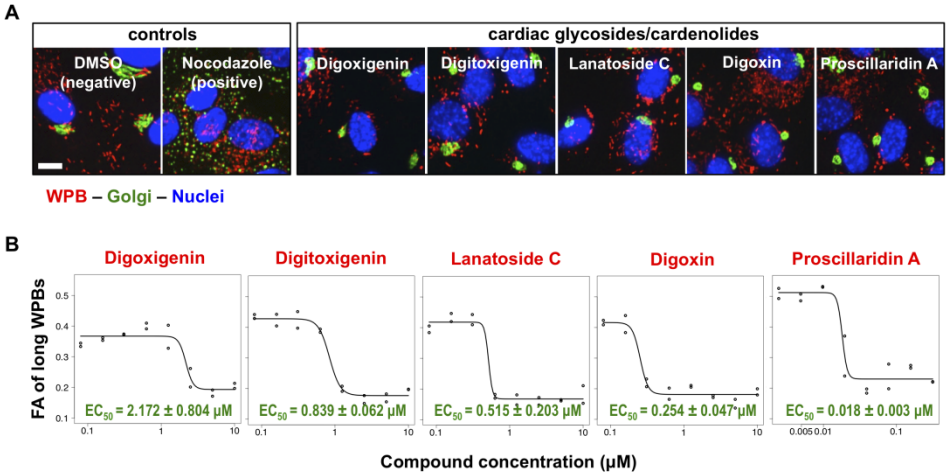

jth_15084_f3.tiff

Figure 4

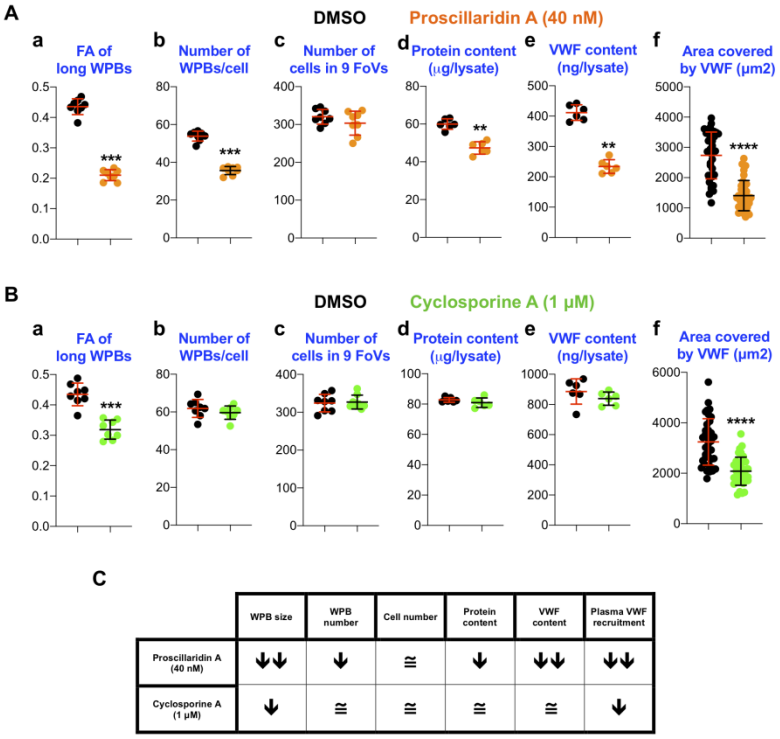

C

	WPB size	WPB number	Cell number	Protein content	VWF content	Plasma VWF recruitment
Proscillaridin A (40 nM)	↓↓	↓	≅	↓	↓↓	↓↓
Cyclosporine A (1 µM)	↓	≅	≅	≅	≅	↓

jth_15084_f4.tiff